THE JOURNAL OF PHYSICAL CHEMISTRY B

ARTICLE

pubs.acs.org/JPCB

The Effect of Mutations on the Alloreactive T Cell Receptor/Peptide−MHC Interface Structure: A Molecular Dynamics Study

Mikhail Y. Wolfson,[†] Kwangho Nam,[*,‡,§] and Arup K. Chakraborty[*,†,∥,⊥,#]

[†]Department of Chemistry, Massachusetts Institute of Technology, Cambridge, Massachusetts 02139, United States

[‡]Department of Chemistry and Chemical Biology, Harvard University, Cambridge, Massachusetts 02138, United States

[§]Department of Stem Cell and Regenerative Biology, Harvard University, Cambridge, Massachusetts 02138, United States

[∥]Department of Chemical Engineering, Massachusetts Institute of Technology, Cambridge, Massachusetts 02139, United States

[⊥]Department of Biological Engineering, Massachusetts Institute of Technology, Cambridge, Massachusetts 02139, United States

[#]The Ragon Institute of MGH, MIT, and Harvard, Boston, Massachusetts 02129, United States

Supporting Information

ABSTRACT: T cells orchestrate adaptive, pathogen-specific immune responses. T cells have a surface receptor (called TCR) whose ligands are complexes (pMHCs) of peptides (derived from pathogens or host proteins) and major histocompatibility complex proteins (MHCs). MHC proteins vary between hosts. During organ transplants, host TCRs interact with peptides present in complex with genetically different MHCs. This usually causes a vigorous immune response: alloreactivity. Studies of alloreactive protein interactions have yielded results that present a puzzle. Some crystallographic studies concluded that the alloreactive TCR/MHC interface is essentially unaffected by changing the TCR peptide-binding region, suggesting that the peptide does not influence the interface. Another biochemical study concluded from mutation data that different peptides can alter the binding interface with the same TCR. To explore the origin of this puzzle, we used molecular dynamics simulations to study the dependence of the TCR/pMHC interface on changes in both the peptide and the TCR. Our simulations show that the footprint of the TCR on the pMHC is insensitive to mutations of the TCR peptide-binding loops, but peptide mutations can make multiple local changes to TCR/pMHC contacts. Therefore, our results demonstrate that the structural and mutation data do not conflict and reveal how subtle, but important, characteristics of the alloreactive TCR/pMHC interface are influenced by the TCR and the peptide.

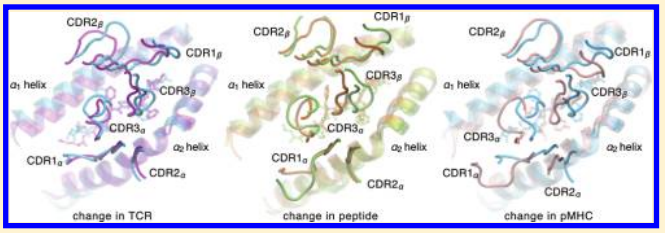

INTRODUCTION

The adaptive immune system enables higher organisms, like humans, to protect themselves with pathogen-specific responses against a diverse and evolving world of microbes. T lymphocytes (T cells) are key orchestrators of the adaptive immune response. To perform their functions, they must be activated. Activation is predicated on sufficiently strong binding of a T cell's antigen receptor (T cell receptor, TCR) to a ligand. The ligand consists of a short peptide fragment held in the cleft of a membrane-bound major histocompatibility complex protein (MHC) displayed on the surface of an antigen-presenting cell. T cell activation can lead to a variety of effector immune functions.

Immature T cells undergo development in the thymus, where they interact with pMHC complexes derived from the host proteome. To survive elimination during the development process, the T cells must not interact too strongly with any of these self-pMHC complexes (negative selection), but must bind with sufficient affinity to at least one pMHC (positive selection).[1−8] This selection process largely inhibits autoimmune T cells from joining the immune system and ensures that the surviving T cells can recognize foreign peptides presented on the host's own MHC molecules with extraordinary specificity.[9,10] Because of thymic selection, peptides derived from the hosts' own proteins do not produce a strong interaction, but foreign-derived peptides do.

Sometimes, such as during organ transplantation, mature T cells encounter pMHC complexes on cells from a genetically different (allogeneic) member of the same species. Since MHC genes are highly polymorphic, allogeneic pMHCs (allo-pMHCs) present previously unseen MHC surfaces to the TCRs. Furthermore, since the most variable regions of the MHC occur along the peptide binding cleft, the peptides presented by allo-MHCs likely differ in sequence and conformation from the self-peptides used to train the TCR in the thymus, even though they originate from the same proteins. Up to 10% of the T cell repertoire can cross-react with any particular pMHC on the allogeneic cells:

Received: March 15, 2011
Revised: April 27, 2011
Published: June 09, 2011

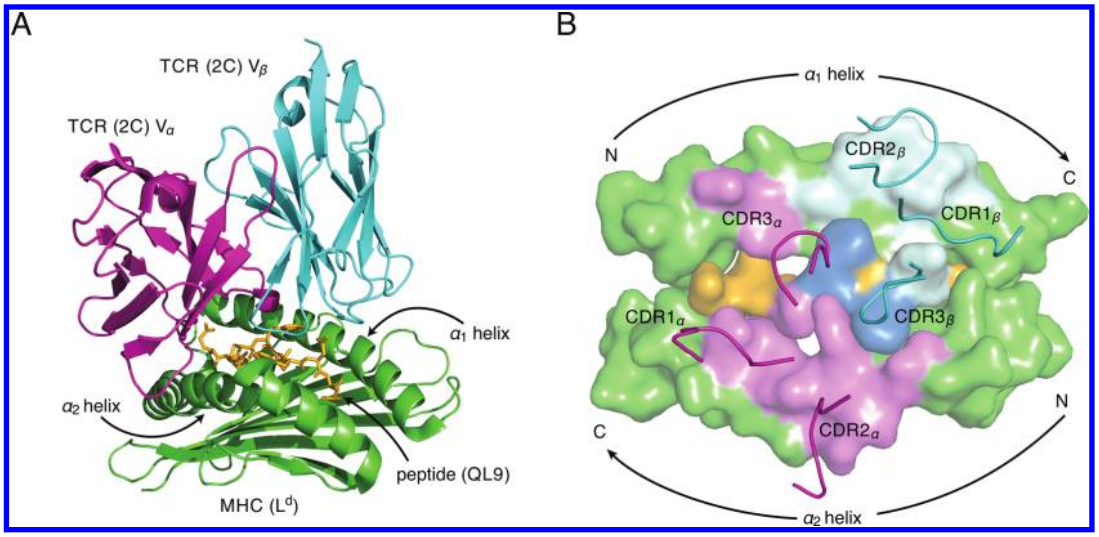

Figure 1. The 2C TCR binds strongly to the allo-MHC L^d, contacting a "footprint" set of residues on the pMHC. A. A crystal structure (PDB 2OI9) of the variable chains of the 2C TCR in complex with the peptide QL9 and the MHC L^d shows the relative orientation of TCR on MHC.[20] B. The diagram of the TCR/pMHC footprint highlights L^d residues that are in contact with 2C. A pMHC residue is considered to be in contact with TCR if it has a non-hydrogen atom within 4.5 Å of a non-hydrogen atom in a TCR residue. pMHC residues that contact the TCR are shaded with the color of the chain(s) they contact: magenta for V_α, cyan for V_β, and dark blue for both. Above the MHC, the 2C CDR loops are indicated in the color of the chain they belong to: magenta for V_α, cyan for V_β. The directionality of the protein backbone is indicated by arrows that point from the amino terminus to the carboxy terminus. Molecular visualizations for this figure were created with PyMol.[21]

1000 times as many T cells as the 0.01% of the repertoire activated during the response to a virus.[11−19] This intense response, known as alloreactivity, makes organ transplantation impossible without immunosuppression.

Much experimental work has been dedicated to elucidating the roles and relative importance of the peptide and MHC in alloreactivity, and a large number of these studies[22−29] have examined the interaction footprint: the interface between the TCR and the set of pMHC residues that come into contact with it, which includes the peptide and the α_1 and α_2 helices of the MHC (Figure 1). A question of particular interest has been the energetic and structural impact of the peptide on an allo-pMHC/TCR footprint. The question has been actively explored by biochemical mutation experiments and X-ray crystallography.

Some biochemical experiments have studied how a TCR interacts with different peptides in the same allo-MHC. But these studies do not provide direct structural data.[30,31] One study, by Felix et al., concluded that peptide mutations could have a noticeable impact on the TCR/pMHC footprint by affecting contacts between MHC and TCR.[30] In the study, the authors mutated several residues along the α-helices of a particular allo-MHC and observed the effects of those mutations on T cell activation, in order to assess which residues were likely to contact the TCR. The authors found that when different peptides were bound by the same allo-MHC, different subsets of MHC residues impacted recognition, implying that the peptides affected the TCR/MHC contacts.

Since the first complete TCR/pMHC crystal structure in 1996,[32] crystal structures have also been used to study several TCR/pMHC footprints. Many of these footprints have been between TCR and peptide/self-MHC complexes,[32−38] but structural studies have dealt with alloreactive complexes as well.[20,39−47] Two of these studies[42,47] have made direct structural comparisons of the effects of different peptides of varying affinity on the TCR/allo-pMHC interface. A recent crystallographic study by Colf et al. concluded that the peptide has little impact on the footprint. The authors reached this conclusion by showing that mutations on the $CDR3_\alpha$ peptide-recognition loop of a TCR bound to an allo-pMHC complex did not impact the structure, despite increasing the binding affinity by over 2 orders of magnitude.[20] Importantly, however, the study did not involve mutation of the peptide itself. A more physical and chemical understanding of the intermolecular interactions involved at the TCR/pMHC interface could shed light on these seemingly conflicting biochemical and crystallographic results. Such insight could also motivate further experiments.

One direct way to compare the two results is to understand a single system that encompasses *both* peptide mutation and structural information. To this end, we have performed an *in silico* analogue of the peptide mutation experiments designed by Felix et al. on TCR/pMHC structures obtained by Colf et al.[20] Using molecular dynamics simulations,[48] we analyzed atomistic models of TCR/allo-pMHC complexes while independently changing both the TCR and the peptide, which allowed us to directly compare the effects of each kind of mutation on the TCR/pMHC interface. In our simulations, as in the crystallographic study, mutation of the $CDR3_\alpha$ loop of the TCR did not induce a significant change in the TCR/allo-pMHC footprint, compared to the significant differences between the TCR/allo-pMHC and TCR/self-pMHC footprints. However, our simulations also showed that certain *peptide* mutations *can* affect the TCR/pMHC interface. These peptide mutations not only affected the peptide−TCR contacts but also influenced which MHC residues came into contact with TCR, even though they did not induce a change in the overall orientation of TCR on MHC: a finding that confirms the conclusions of Felix et al.[30] Our simulations thus demonstrate that the crystallographic results and biochemical results are not in conflict, because mutations to the $CDR3_\alpha$ loop are not necessarily equivalent to peptide mutations. Our results highlight the potential of the

Table 1. Lower-Affinity Peptide Mutants Are Good Candidates for Simulation

Peptide[a]	Sequence	TCR/pMHC K_a (M^{-1})[b]	Reference
QL9	QLSPFPFDL	$1.0 - 2.0 \cdot 10^7$	67
QL9-A6	QLSPFAFDL	$2.0 \cdot 10^5$	68
p2Ca	-LSPFPFDL	$2.0 \cdot 10^6$	67
p2Ca-A5	-LSPFAFDL	$1.6 \cdot 10^4$	67

[a] In order to assess the impact of peptide mutations on the TCR/pMHC footprint, we chose to simulate the 2C/QL9-L^d system with several lower-affinity peptide variants. The table lists sequences and binding affinities of these peptides. The mutants were chosen to impact the binding affinity by at least a factor of 5, so as to not simulate "null" mutations. [b] Binding affinities were obtained from solution measurements of peptide on L^d, presented to 2C.

peptide to impact the TCR/pMHC interface by making local contact changes and suggest that detailed chemical interactions at the interface between the TCR, peptide, and MHC can all play a part in the ultimate structure of the alloreactive TCR/pMHC interface.

Our findings are consistent with an attractive model for TCR/pMHC interactions in which the TCR docks over the pMHC and scans the ligand for a sufficient number of interactions that confer on the TCR/pMHC complex a sufficient lifetime.[8,49−51] If this necessary condition for recognition is met, structural rearrangements occur to acquire enhanced affinity. The specific character of these relatively modest rearrangements[29] depends on the particular TCR/pMHC pair under consideration.

METHODS

Structure Preparation. The X-ray structures of the C9X and M9X[20] complexes (PDB IDs 2OI9 and 2E7L, respectively) were used for the initial coordinates of all calculations. Three mutant-peptide variants were generated from each crystal structure by removing the atoms that corresponded to the mutation (Table 1). This resulted in a total of eight systems to simulate. Hydrogen atoms were introduced into the structures with a stereochemical algorithm.[52] The protonation states of titratable residues were assigned based on visual inspection and prior results for similar systems.[53−55] The structures were minimized with constraints on heavy atom positions and solvated with explicit TIP3P[56,57] water molecules in 89 Å rhombic dodecahedra with periodic boundary conditions. 39 K^+ ions and 37−38 Cl^- ions were added to each system to neutralize the total charge and simulate a 0.15 M KCl concentration. The ions were placed with random initial coordinates, then subjected to 2000 steps of a Metropolis Monte Carlo simulation in order to equilibrate their positions. After solvation, hydrogens, solvent atoms, and protein atoms were all minimized with restraints in stages. First, hydrogens were minimized for 1000 steps without restraints, while heavy atoms were fixed. Then, only the solvent atoms were subjected to 1000 additional steps of restrained minimization, with force constants of 0.5 kcal/mol/Å^2, while protein atoms were fixed. After that, all atoms were unfixed, a 0.1 kcal/mol/Å^2 harmonic restraint was placed on the protein atoms, and the system was subjected to 1000 more steps of minimization. Finally, the entire system was minimized again for 1000 steps without restraints. The average number of atoms per system was 47,355.

Molecular Dynamics Simulations. All simulations were performed using the CHARMM[58,59] molecular dynamics program (version c34b1) with the CHARMM22[56] force field and the CMAP correction for the peptide backbone dihedrals.[60] The simulation protocol was influenced by previous TCR/pMHC simulations.[53−55] Molecular dynamics simulations were performed with holomorphic constraints on the hydrogen atoms,[61] which allowed the use of 2 fs integration timesteps. Nonbonded van der Waals interactions were truncated at 9 Å using a force-switching algorithm.[62] Electrostatic terms were calculated using the particle-mesh Ewald summation method,[63] and the real-space terms were evaluated with a 9 Å cutoff. After solvation and the energy minimizations described above, each system was heated and equilibrated in several stages. First, the entire system was heated from 10 to 300 K over 100 ps without restraints. Then a 3.0 kcal/mol/Å^2 harmonic restraint was placed on the heavy protein atoms, and the ions and solvent were equilibrated with three repetitions of a heating and cooling cycle. The cycle ran constant-temperature dynamics for 50 ps at 300 K, then heated the system to 450 K, ran constant-temperature dynamics for 100 ps, cooled the system down to 300 K, then ran another 100 ps of constant-temperature dynamics at 300 K. After the solvent equilibration, a mass-weighted 0.75 kcal/mol/Å^2 harmonic restraint was placed on protein heavy atoms and the system was equilibrated for 100 ps with constant-temperature dynamics. The restrained dynamics were followed with 100 ps of unrestrained constant-temperature dynamics, and 200 ps of unrestrained constant-temperature, constant-pressure dynamics. Simulations were then continued for 15 ns. Throughout each simulation, constant temperature was maintained with the Nosé−Hoover thermostat,[64,65] and constant pressure was maintained with the Langevin piston method.[66]

RESULTS

Alloreactive Model. The alloreactive model used in our simulations is based on the murine 2C TCR. T cells containing this TCR were found in a mouse—whose own MHC molecules expressed the K^b-haplotype—injected with cells whose MHCs had the L^d haplotype.[69,70] Thus, 2C TCRs recognize foreign and self-peptides on the K^b self-MHC and also bind strongly to peptides presented on the L^d allo-MHC (Figure 1). Crystallographic experiments by Colf et al.[20] have obtained the structure of the variable part of a 2C TCR in contact with a peptide (QL9; see Table 1 for sequence) held in the cleft of a stabilized portion of L^d (α_1/α_2 domains, residues 1−180 of the heavy chain). The crystal structure of the same ligand bound to m6, a mutant of 2C with even higher affinity for QL9/L^d, was also obtained. The only difference in sequence between 2C and m6 occurs in residues 94−103 of the CDR3$_\alpha$ loop, which is changed from the sequence GFASA in 2C to the sequence HQGRY in m6. Despite the 100-fold change in affinity for the ligand caused by this mutation, it had no significant impact on the TCR/pMHC footprint, especially when compared to the structural difference between the 2C/QL9-L^d structure and previously obtained 2C/K^b self-pMHC structures.[20,33] This result led Colf et al. to conclude that the peptide did not play an important structural role in the footprint because, even though interactions between the peptide and TCR had significantly changed, the footprint had not.

Molecular Dynamics Simulations. To study the effect of both TCR and peptide mutation on the TCR/pMHC footprint, we performed molecular dynamics simulations on a total of eight

Table 2. Abbreviations Used for the TCR/pMHC Systems Discussed in This Article

peptide	TCR	MHC	source	abbreviation[a]
QL9	2C	L^d	dynamics	C9P
	m6	L^d	dynamics	M9P
	2C	L^d	structure	C9X
	m6	L^d	structure	M9X
QL9-A6	2C	L^d	dynamics	C9A
	m6	L^d	dynamics	M9A
p2Ca	2C	L^d	dynamics	C8P
	m6	L^d	dynamics	M8P
p2Ca-A5	2C	L^d	dynamics	C8A
	m6	L^d	dynamics	M8A
SIYR	2C	K^b	dynamics	CSK
	2C	K^b	structure	CSX

[a] The abbreviation code describes the distinguishing features of a system with three characters. For the L^d simulations, the first character describes the TCR involved: "C" for 2C, "M" for m6. The second character describes how many amino acids are in the peptide: "9" for QL9 and its mutants, "8" for p2Ca and its mutants. The third character describes the variation. If the abbreviation refers to a simulated structure, "P" stands for the peptides with proline at position 5 or 6, QL9 and p2Ca, and "A" stands for the alanine mutants QL9-A6 and p2Ca-A5. The third character can also be "X," which is a special case indicating that the abbreviation refers to a crystal structure. Finally, the K^b systems are named in a manner to mimic consistency with the L^d systems: "C" for 2C, "S" for the SIYR peptide, "K" for K^b, and "X" for the crystal structure.

systems. For the peptide mutants, we used four peptides (Table 1), including QL9. The three additional peptides were derived from QL9 by independently introducing two mutations: deletion of the terminal glutamine, and mutation of the carboxy-proximal proline to an alanine. These mutations were chosen for their ability to noticeably affect the binding affinity of the peptide for 2C.[67,68] Each of the four pMHCs was simulated with both 2C and m6 TCR, with the m6 simulations intended to test the effect of TCR mutation. The simulated systems are summarized in Table 2, along with their identifying abbreviations.

Since the peptide mutations involved only removal of atoms, the initial coordinates of the mutant peptides were the same as the crystal coordinates of QL9, except for the deleted atoms. The molecular dynamics simulations were carried out for 15 ns, and coordinates were saved at every 2 ps for analysis. Energetic and structural properties of the systems were calculated by averaging over the last 5 ns of the trajectories, after the systems had reached equilibrated states. Equilibration was determined by a consistent plateau in the rmsd (root-mean-square deviations) of the backbone coordinates from the crystal structure (Figure 1 in the Supporting Information). The binding free energy of the m6 TCR for pMHC was calculated to be stronger (more negative) than that of 2C (Table 1 in the Supporting Information), which corresponds qualitatively to experimental binding affinity measurements.[44]

To provide more points of reference, a model of the 2C/K^b system was also simulated. The resolution of the crystal structure referenced by Colf et al., originally obtained by Garcia et al.,[33] was not high enough for consistent simulations. Instead, a related structure, which replaced the original dEV8 self-peptide with the superagonist SIYR peptide, was used.[35] This structure had a higher resolution, yet differed little (rmsd 0.92 for C_α atoms) from the original 2C/K^b/dEV8 structure and could therefore serve as an approximate model.

Average Structures from the Dynamics Highlight the Overall Effect of Peptide Mutation. In order to evaluate the qualitative effects of peptide mutation, we calculated average TCR/pMHC structures from each trajectory by taking the mean position of each atom during the last 5 ns of the trajectory. Figure 2 displays some of these average structures superimposed on one another for comparison. The structures in each part of the figure are aligned along their MHC backbone atoms to highlight differences in TCR loop position and TCR/MHC orientation. Figure 2 is designed to show the effect of TCR mutation (Figure 2A), the effect of peptide mutation (Figure 2B), and the effect of switching from self-pMHC to allo-pMHC (Figure 2C). Looking from Figure 2A to Figure 2C, the differences between the structures in each pair increase. In Figure 2A, the qualitative features Colf et al. found are reproduced: the overall orientation of both TCRs is nearly identical,[20] despite a few minor loop rearrangements, leading to an average backbone rmsd of 2.7 Å for the loops. By stark contrast, in Figure 2C, almost all of the TCR loops have significantly different average positions, with an average backbone rmsd of 3.5 Å,[29] and it is clear that 2C binds to the different pMHCs at different angles. Figure 2A and Figure 2C together demonstrate that our simulations retain qualitative similarity to the crystallographers' finding that CDR3 loop mutation is insignificant, especially compared to the differences between self- and allo-pMHC.[20] Figure 2B shows how the effects of peptide mutation compare with the two "extremes" of Figure 2A (no effect) and Figure 2C (drastic effect). The two peptide mutant systems shown in this subfigure, C8A and C8P, exhibit the greatest difference from one another among all choices of peptide mutants for a given TCR, highlighting the maximum observed extent of peptide mutation. Comparing C8A to C8P shows that, although there is no global rearrangement of binding orientation, as in Figure 2C, there are many differences between the conformations of the 2C CDR loops, and the differences are distributed throughout most of the CDR loops, yielding an average backbone rmsd of 3.4 Å. Every loop except $CDR2_\alpha$ exhibits a noticeable difference between the two structures. These unique loop conformations lead to significantly different TCR/pMHC contacts. In particular, the most significant differences are seen in the CDR3 loops, which contact the peptide directly. The peptides, however, are not adopting vastly different conformations (backbone rmsd 1.9 Å). This result suggests that the peptides interact with the TCR in a highly dissimilar manner despite their relatively similar orientation and that mutation can affect the TCR/pMHC contacts through a complex interplay of altered interactions between the TCR and the bound pMHC.

TCR/pMHC Contact Distributions Allow Quantitative Comparison of the Effects of Mutation. To measure the impact of peptide mutations on the footprint, we computed the number of contacts that each pMHC residue makes with TCR and averaged these quantities over the structures obtained during the last 5 ns of simulation. We defined any two residues to be in contact when a non-hydrogen atom in one residue was within 4.5 Å of a non-hydrogen atom in the other residue. This average-contact approach qualitatively differs from analyzing any single "representative" structure taken from the simulation trajectory, since a single structure may not accurately represent the overall ensemble of structures well enough, especially when

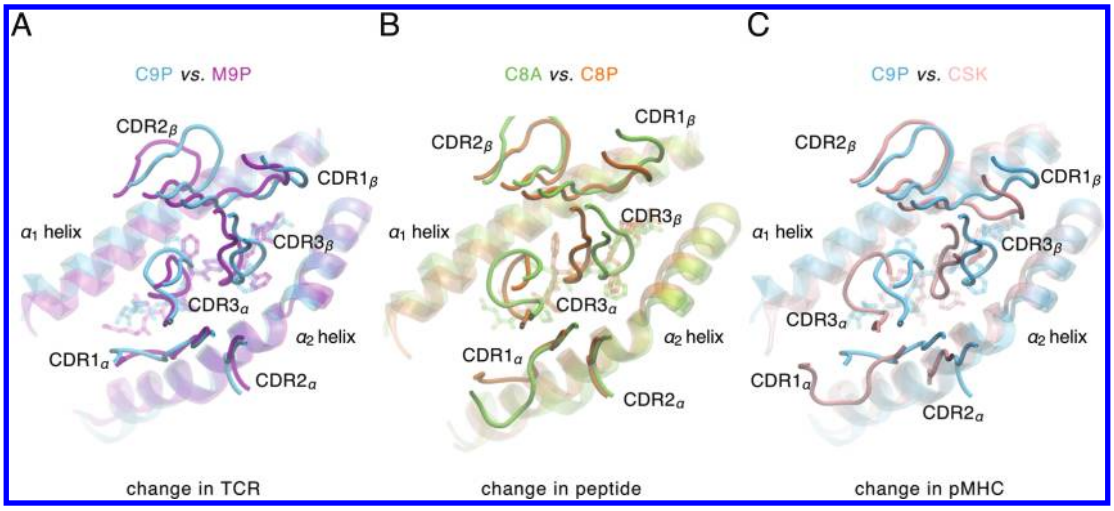

Figure 2. Average structures of the TCR/pMHC footprints compare the effects of TCR, peptide, and pMHC changes. The comparison highlights the ability of the simulations to reproduce qualitative experimental results. The average structures are aligned via their MHC backbone atoms to allow comparisons between TCR loop displacement and TCR orientation. The differences between the two structures are most noticeable in C, and least pronounced in A, in agreement with experimental results. B, which highlights differences from peptide mutation, shows differences that lie between the two extremes. The average structures were obtained from the 5 ns of the trajectories, with rotation and translation removed. Molecular visualizations for this figure were created with VMD.[71]

examining the contact footprint. Thus, an analysis based on a single structure would likely suffer from ambiguities in interpreting the results.

The result of the average contact calculations, shown in Figure 3 and Figure 4, is a picture of the interaction footprints as functions of pMHC sequence. In each plot, the ordinate lists the positional indices and amino acid abbreviations for the residues that constitute a particular segment of the pMHC: either the α_1 helix or the α_2 helix. Around each point, which represents an individual pMHC residue, a group of bars is clustered. The set of all bars of a single color represents a particular TCR/pMHC system, as described by the legend and Table 2, and the length of a bar represents the average number of contacts that a pMHC residue made with TCR. Figure 4 shows the effect of peptide mutation on the 2C footprint by comparing all simulated systems that involve the binding of 2C TCR to different peptides: C9P, C9A, C8P, and C8A, respectively. Figure 3 serves as a control by comparing the footprints of the 2C and m6 crystal structures (C9X, M9X) with their corresponding simulations (C9P, M9P). The control set provides two methods of testing the simulations against experimental results, showing (1) how well the simulations reproduce the experimental conclusions that mutation from 2C to m6 does not have a significant effect on the footprint, and (2) how similar the footprints generated by the simulations are to their experimental counterparts. To be numerically significant, any changes observed from peptide mutation would have to be larger than the differences between crystal structures and their simulation counterparts, and also larger than the differences between the 2C and m6 TCR simulations.

Figure 4 directly shows how peptide mutation changes local contacts between MHC residues and TCR in several locations throughout the footprint, in direct support of the findings of Felix et al.,[30] that peptide mutations can rearrange the finely paired contacts between TCR and MHC. For a more quantitative comparison of the footprints, we present a single system's footprint (the set of all bars of the same color) as a discrete "distribution" of contacts over the sequence of the pMHC. The distributions of different systems can be compared segment-by-segment by their "means," $\bar{r}_c$, shown in Figure 5. The $\bar{r}_c$s are calculated as weighted averages,

$$\bar{r}_c(A;\mathbb{S}) = \frac{\sum_{r \in \mathbb{S}} c(r) r}{\sum_{r \in \mathbb{S}} c(r)} \quad (1)$$

where $\mathbb{S} \in \{\alpha_1,\alpha_2,\text{pep}\}$ is a label for a pMHC segment (either the α_1 helix, the α_2 helix, or the peptide) of a TCR/pMHC system A, r is the sequence number of a residue in $\mathbb{S}$ (denoted along the ordinate), and $c(r)$ is the average number of contacts that residue r makes with TCR (the length of the bar at position r that corresponds to system A in Figure 3 and Figure 4). Thus, $\bar{r}_c(A;\mathbb{S})$ represents the average position in the sequence where the TCR contact distribution for pMHC segment $\mathbb{S}$ is centered in system A, i.e. the contact center of mass. Differences between the means of two distributions representing different systems reflect underlying differences between the TCR/pMHC contact distributions of those systems (Figure 5), and we will use the notation $\Delta\bar{r}_c(A_1 - A_2;\mathbb{S}) \equiv |\bar{r}_c(A_1;\mathbb{S}) - \bar{r}_c(A_2;\mathbb{S})|$ to refer to these differences throughout the paper.

Mutations to the CDR3$_\alpha$ Loop of the TCR Do Not Produce Significant Changes to the Footprint. To verify the predictive quality of the simulations, we first examined how well they reproduce the experimental result that CDR3 mutations do not significantly alter the footprint.[20] Figure 3 and Figure 5 compare the contact distributions and $\bar{r}_c$s of C9P to M9P, and C9X to M9X—an intramethod, inter-TCR comparison—to assess the effect of the TCR mutation (2C → m6) on TCR/MHC contacts. The contact distributions of the crystallographic C9X and M9X systems are very similar to one another, except for a few stray contacts in M9X near the ends of the helices and two contacts with Arg75 of the MHC, which are only present in the C9X structure (Figure 3). Like their crystallographic counterparts, M9P and C9P are also similar to one another, as reflected by the small difference in their $\bar{r}_c$s (Figure 5). However, M9P has

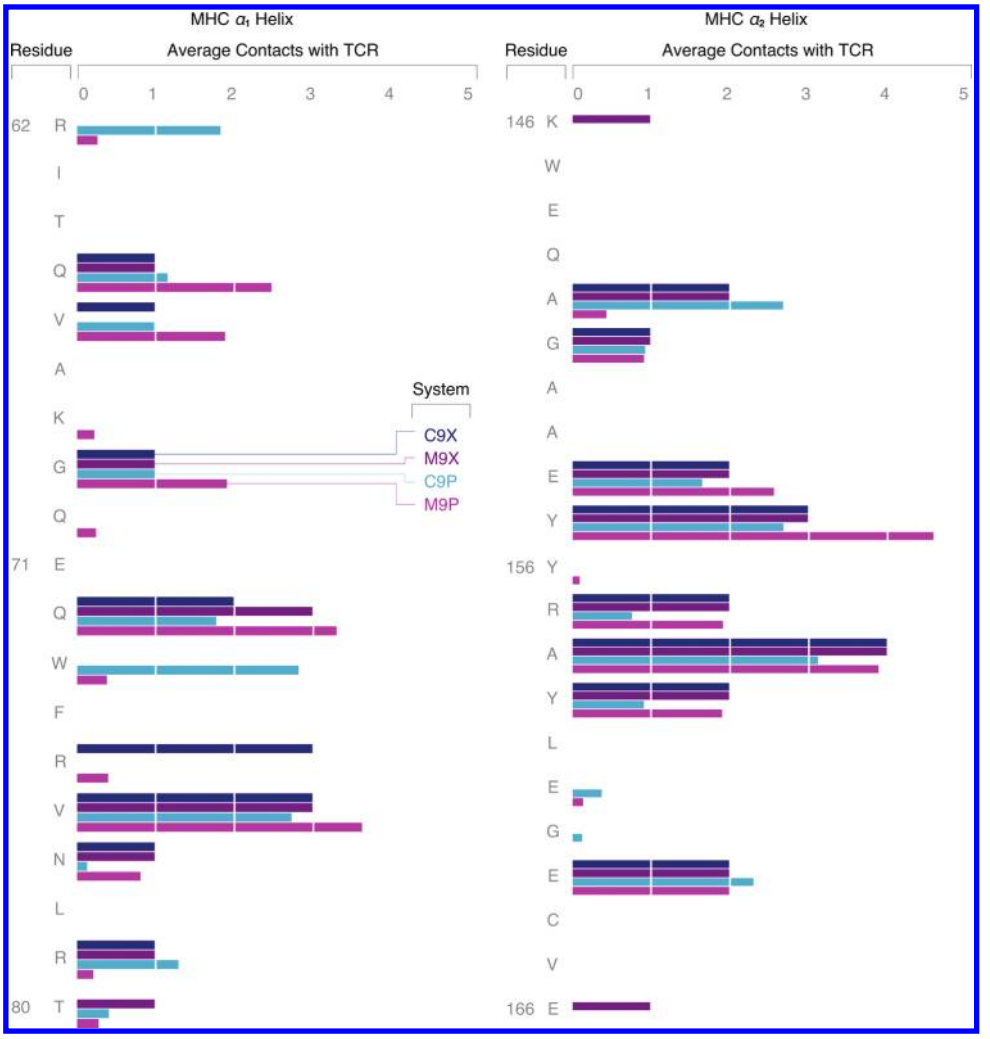

Figure 3. MHC/TCR contact distributions show a quantitative description of the TCR/pMHC footprint. The figure compares the crystal structure footprints to their corresponding simulations in order to establish the accuracy of the simulations. In general, the simulations reproduce the result that mutation of the TCR does not make widespread changes to the footprint. The ordinate axes list the residue index and single-letter amino acid abbreviation for the residues of the MHC α_1 and α_2 helices. For the simulations (C9P and M9P), the length of each bar represents how many contacts, on average, that MHC residue made with any TCR residue during the last 5 ns of the dynamics trajectory. For the crystal structure data (C9X and M9X), the length of a bar represents the exact number of contacts observed in that structure. Two residues were defined to be in contact if a non-hydrogen atom in one residue was within 4.5 Å of a non-hydrogen atom within another. SEM error for each bar length was calculated but is too small to be visible.

approximately one more average TCR contact than C9P in several places where MHC/TCR contacts already exist in C9P. The additional average contacts are distributed almost evenly throughout the entire contact interface. Due to the normalization applied in eq 1, this difference is not reflected in the $\Delta\bar{r}_c(\text{M9P};-\{\alpha_1,\alpha_2\})$ values, and therefore, no significant shift is observed in the location of the footprint on the MHC. The even distribution of additional contacts suggests that the m6 TCR interacts strongly with the pMHC. This is consistent with the experimental finding that the m6 TCR has a higher affinity for the L^d-QL9 ligand[20] and with the computed binding free energies reported in Table 1 in the Supporting Information.

As a further test of quality, we compare the QL9 simulations (C9P and M9P) to their corresponding crystal structures (C9X and M9X)—the only direct experimental comparison available—in the bottom of Figure 5. This intermethod, intra-TCR comparison yields larger differences in $\bar{r}_c$ between simulation and experiment than the previous comparison, especially for the α_1 helix. The differences may reflect the large numbers of crystal contacts (476 crystal contacts for C9X and 874 for M9X), that are present only in the crystal structures and are absent in our simulations. Further analysis shows that, in the α_1 helix, 74% of $\Delta\bar{r}_c(\text{C9P}-\text{C9X};\alpha_1)$ is due to the two TCR contacts with residue Arg62 on the α_1 helix of the MHC which develop in the C9P simulation, but are absent in the C9X structure. Other contact patterns are mostly conserved between simulation and experiment. Since such a large part of the difference can be accounted for by only one new contact location, the difference in $\bar{r}_c$s does not reflect the widespread shifts in pMHC contact locations that would accompany a significant change in the footprint. Although the intermethod $\Delta\bar{r}_c(\text{M9X}-\text{M9P};\alpha_1)$ is larger than $\Delta\bar{r}_c(\text{C9X}-\text{C9P};\alpha_1)$, and both are relatively large, they are still smaller than the largest $\Delta\bar{r}_c$ obtained from peptide mutation and therefore do not affect qualitative conclusions about its potential effects.

The smaller size of both of the intramethod, inter-TCR comparison $\Delta\bar{r}_c$s, relative to the intermethod, intra-TCR $\Delta\bar{r}_c$s,

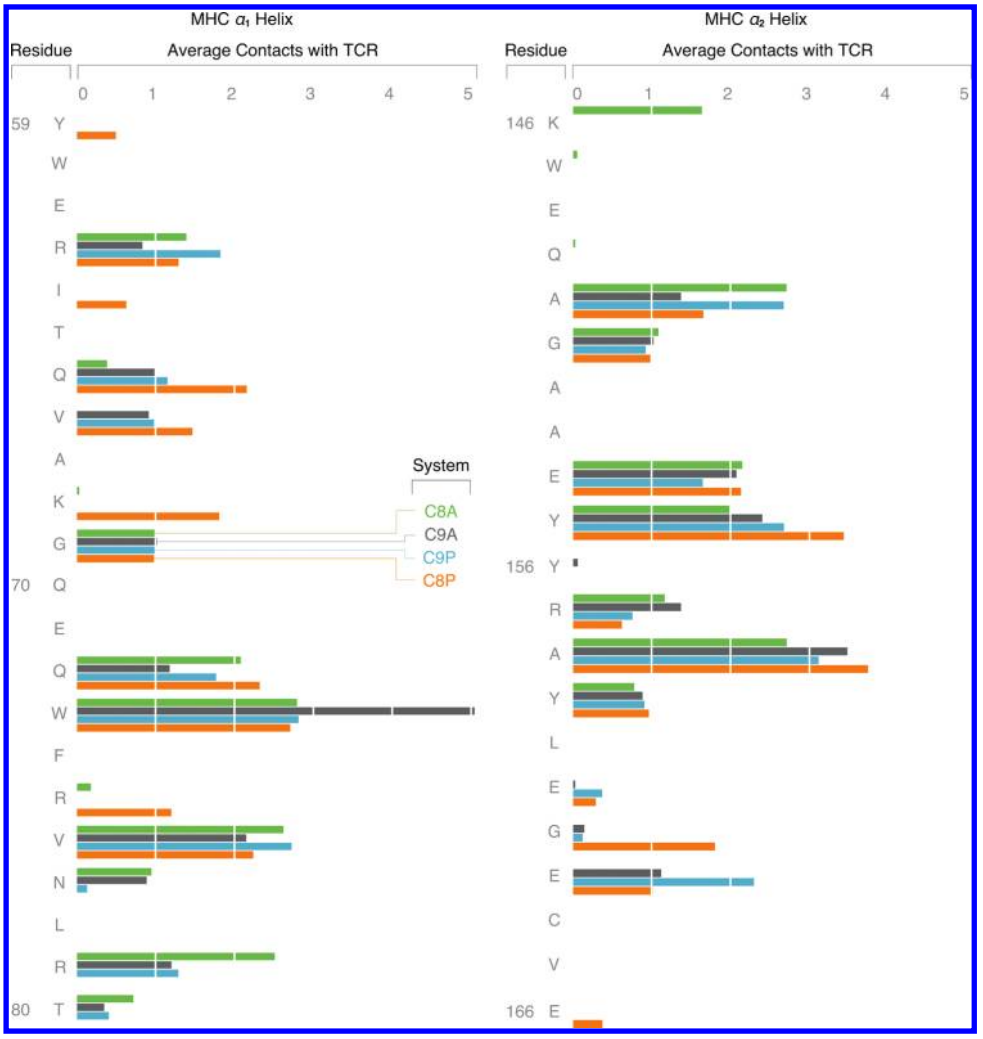

Figure 4. Peptide mutation can induce local TCR/MHC contact changes. MHC/TCR contact distributions of peptide mutant systems show the effects of peptide mutation on the interface. Some of these effects are significant: the C8A distribution is noticeably different from the C8P distribution. The ordinate axes list the residue index and single-letter amino acid abbreviation for the residues of the MHC α_1 and α_2 helices. The length of each bar represents how many contacts, on average, that MHC residue made with any TCR residue during the last 5 ns of the dynamics trajectory. Contacts were defined the same way as in Figure 3. SEM error for each bar length was calculated but is too small to be visible.

suggests that the simulations and crystal structures might have systematic, localized shifts from one another. Such systematic shifts may be caused, for example, by the absence of crystal contacts in the simulations. The two comparisons, taken together, suggest that, despite some localized differences with the crystal structures, our simulations are consistent with the experimental result that mutation of the 2C CDR3$_\alpha$ loop does not induce significant perturbations in TCR/MHC contacts with QL9-L^d.

Mutations to the Shortened Antigenic Peptide Produce Noticeable, Local Changes to TCR/MHC Contacts. Among all the peptide mutant systems tested, two (C8P and C8A) show the largest shifts in $\bar{r}_c$ values, larger than any other pair of systems with the same TCR by at least a factor of 2 (Figure 5). The exact $\bar{r}_c$ values that underlie these differences are shown in Table 2 in the Supporting Information.

Unlike the case of TCR mutation, the simple creation or annihilation of a single MHC/TCR contact cannot account for the large shift in $\bar{r}_c$. Rather, the shift is caused by the rearrangement of several contacts and an overall shift in the contact distributions of C8A and C8P to opposite ends of the sequence (relative to the wild-type C9P). This can be seen clearly in Figure 2B, where the CDR1 and CDR3 loops for both V$_\alpha$ and V$_\beta$ have noticeably different average conformations in C8A than they do in C8P.

We also determined how widely distributed along the MHC the differences between C8P and C8A are (Figure 5). When comparing two footprints, we define a pMHC site as "changed" if it has 1.0 or more average contacts in one footprint, and 0.5 average contacts or less in the other. This choice of cutoff values is reasonable, as a pMHC residue with less than 0.5 average TCR contacts makes no contact with TCR more than half the time, but a pMHC residue with 1.0 average TCR contacts is in contact with the TCR on average once every time step in the trajectory. Using the above definition of change to compare C8A to C8P yields 8 changed sites out of 22, while comparing C9P to C9X or C9P to M9P yields only 4 out of 21 sites. The results are not very sensitive to changes of the cutoff values: if either parameter were varied by up to 10% in either direction, only two changed sites would lose their label, and in both cases, it is because the high

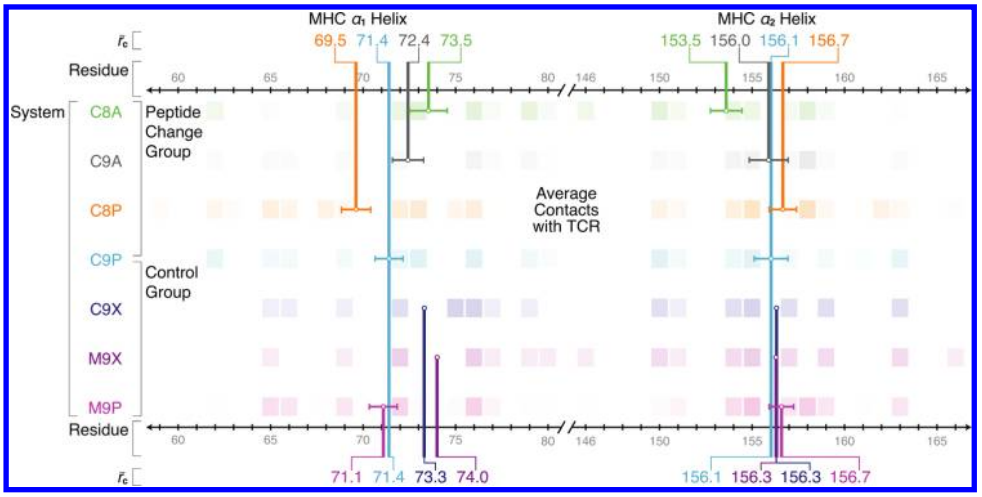

Figure 5. The changes in TCR/MHC contacts upon peptide mutation from C8P to C8A are numerically significant. The values of $\bar{r}_c$ for each system are plotted above on the same axes for comparison. $\bar{r}_c$ represents the "center of mass" of the contact distributions, and the difference induced in $\bar{r}_c$ by peptide mutation from C8P to C8A is clearly bigger than the difference between any systems in the control group. Between the $\bar{r}_c$ axes, a color-coded picture of the contact distributions in Figure 3 and Figure 4 is shown, in order to provide a qualitative picture of "contact mass": the more brightly colored a particular square is, the more contacts with TCR it makes. Errors signified by error bars emanating from the circular data points are in SEM, except for the crystallographic C9X and M9X systems.

value is very close to 1.0, and would cease to qualify as a contact if the upper threshold were raised to 1.1. The comparatively large number of changed sites demonstrates that differences between the C8A and C8P footprint are widely distributed and represent changes throughout the footprint.

Figure 5 also shows that the wild-type C9P contact distributions are centered between those of the C8P and C8A systems for both MHC helices. Thus, relative to the original, wild-type footprint, the lone deletion (C8P) and deletion-with-mutation (C8A) have opposite, nonadditive effects, possibly due to how greatly deletion can affect the space available to the peptide. Taken as a whole, these effects are relatively localized to the TCR−MHC interface, and they do not involve the kind of structural rearrangement of TCR/MHC orientation observed when comparing the allo 2C/QL9-L^d (C9P) to 2C/SIYR-K^b (CSK) (Figure 2C), nor do they involve large rearrangement of the CDR loops themselves. This perspective is consistent with assessments of TCR/pMHC interfaces that highlight the relative inflexibility of the CDR loops.[28,29] Nevertheless, it is clear that mutation of the antigenic peptide, unlike mutation of the $CDR3_\alpha$, can induce noticeable rearrangement of local contacts in the footprint.

Most importantly, these peptide mutation results are completely consistent with the findings of Felix et al.,[30] which implied that changing the peptide can make changes to contacts between MHC and TCR throughout the footprint. They are also consistent with a previous crystallographic study of dissimilar peptides in the same TCR/allo-MHC complex.[42] Performing $\bar{r}_c$ calculations on the crystal structures compared in that study showed that the contact distributions of the different peptide mutants differed by as much as two residue positions: much more than C9X differed from M9X (Table 2 in the Supporting Information).

Recent crystal structures obtained by MacDonald et al.[47] show the LC13 TCR in complex with different peptides in the same allo-MHC. In both cases, the TCR produces a remarkably similar footprint on the substrate. In this situation, however, no residues were removed from the peptide, so the physical impact of mutation was not as severe, despite several sequence differences between the two peptides. Such results indicate that not all kinds of peptide mutation are equivalent: while allopeptide mutations can have an impact on the TCR/pMHC footprint, this is not necessarily the case for a particular TCR/pMHC pair and a particular mutation; in the end, the specific interplay of TCR, peptide, and MHC interactions determines the ultimate interface structure.

Peptide Mutations Can Impact the Topology of the Interface by Changing the ratio of TCR V_α and V_β Chain Contacts. A particular feature of the 2C contact distributions is that the ranking of $\bar{r}_c$ values for the α_1 helix is the inverse of the ranking for the α_2 helix. That is, $\bar{r}_c(C8A;\alpha_1) > \bar{r}_c(C8P;\alpha_1)$, but $\bar{r}_c(C8A;\alpha_2) < \bar{r}_c(C8P;\alpha_2)$ (Figure 5). Since the sequence of the MHC α helices is organized in such a way that the N-terminus of one helix is close in space to the C-terminus of the other helix and *vice versa* (Figure 1), what appears as shifts in opposite directions along the sequence actually corresponds to a shift of the contact footprints in the same direction in space. Specifically, the shifts indicate that, for C8P, more TCR contacts occur on the part of the MHC near the N-terminus of the peptide (the left end in Figure 1B), while for C8A, more TCR contacts occur on the part of the MHC near the C-terminus of the peptide (the right end in Figure 1B). The more space available to 8-mer peptides may allow this "rocking" flexibility, as is discussed in the following section.

From the diagram of the footprint in Figure 1B, it is clear that the chain of the TCR is oriented closer to the C-terminal end of the α_2 MHC helix (on the right in the figure), and the V_β chain of the TCR is oriented closer to the C-terminal end of the α_1 helix (on the left in the figure). Combining this structural knowledge with the contact data discussed above, we expect that C8P would contain more MHC contacts with V_α, and C8A would contain more MHC−V_β contacts. In other words, the change from C8P to C8A would increase the ratio of V_β to V_α contacts. Table 3 shows that this is the case. In C8P, L^d makes 27 contacts with V_α and 21 contacts with V_β, while in C8A, L^d makes only 15 contacts with V_α and 23 contacts with V_β. The changes result in a shift

dx.doi.org/10.1021/jp202471d |J. Phys. Chem. B 2011, 115, 8317–8327

Table 3. Peptide Mutation Can Affect the Ratio of V_β/V_α Contacts with pMHC

system	av V_α/pMHC contacts	av V_β/pMHC contacts	ratio V_β/V_α contacts[a]
C9P	23.57 ± 0.06	16.91 ± 0.05	0.71 ± 0.08
C9A	23.20 ± 0.05	15.89 ± 0.07	0.68 ± 0.09
C8P	26.54 ± 0.06	21.17 ± 0.05	0.79 ± 0.08
C8A	15.41 ± 0.06	22.55 ± 0.06	1.46 ± 0.08
M9P	29.85 ± 0.05	19.03 ± 0.07	0.63 ± 0.09
C9X	25	23	0.92
M9X	27	22	0.81

[a] In C8A, TCR contacts with pMHC are biased toward the V_α chain, while in C8P, they are biased toward the V_β chain. The difference between average V_α contacts between C8A and C8P is larger than any of the differences obtained from comparing corresponding simulation and crystal structure data, or from comparing C9P to M9P. Errors reported are SEM.

of the V_β/V_α ratio from 0.79 to 1.46 as C8P changes to C8A. Figure 2 provides a structural explanation of the drop in V_α contacts, showing that, in C8A, the $CDR1_\alpha$ loop tends away from the MHC, unlike in C8P.

These results demonstrate how the mutation of the fifth position of the shortened peptide from a proline to an alanine (C8P → C8A) can cause rearrangement of the contact topology, affecting not only which MHC residues come into contact with TCR but also which TCR residues contact the MHC.

Mutations to the 9-mer Peptide Produce Less Contact Rearrangement than Mutations to the 8-mer Peptide. By looking at all four peptide variants together, we can compare the relative impact of the mutation of the Ala6/5 residue on the footprint in both the 9-mer and 8-mer peptides. When we compare $\Delta\bar{r}_c(\text{C8A}-\text{C8P};\{\alpha_1,\alpha_2\})$ to $\Delta\bar{r}_c(\text{C9A}-\text{C9P};\{\alpha_1,\alpha_2\})$, it is clear that the footprint is significantly more sensitive to mutation at the Ala5 position of the 8-mer peptide than it is to mutation at the corresponding Ala6 position of the 9-mer peptide. While mutation of the 9-mer peptide does change contacts throughout the footprint, these changes do not affect the values of $\bar{r}_c(\text{C9P};\{\alpha_1,\alpha_2\})/\bar{r}_c(\text{C9A};\{\alpha_1,\alpha_2\})$ more than inherent differences between crystal structure and simulation. Thus, although they may be due to underlying differences in the contact interface, these differences are not large enough to be seen as significant.

The shorter peptide evidently allows more freedom for the α helices—and thereby the entire footprint—to rearrange in response to a mutation in the center of the peptide. Despite such rearrangement, the mutation seems to have a similar effect on TCR binding in both the 8-mer and 9-mer peptide systems, lowering the TCR/pMHC affinity by 2 orders of magnitude (Table 1). This lack of correlation between binding affinity changes and structural rearrangement may seem counterintuitive, but it is in fact consistent with other results that describe sets of nearly identical TCR/pMHC crystal structures with highly varying TCR binding affinities.[34]

The structural distinction that the footprint makes between mutations to the shortened and full-length peptide suggests that TCR and allo-pMHC have a complicated interaction landscape at their interface and therefore can respond to subtle changes in unique ways.

DISCUSSION

The intent of our study has been to provide insight into the structural impact of peptide mutations on the alloreactive TCR/pMHC interface by comparing atomistic models of systems that have not yet been crystallized. In our simulations, mutation of the TCR's $CDR3_\alpha$ loop did not induce significant rearrangement of the TCR/MHC contacts, but certain mutations of the peptide made noticeable changes to local contacts throughout the TCR/pMHC interface.

Our results contribute to a large body of work aimed at elucidating the nature of the 2C TCR alloreactive response in particular and alloreactive responses in general. That work has yielded two differing pictures of the peptide's structural influence on the TCR/pMHC footprint: a peptide-centric model,[22,30,31,37] in which the peptide plays an important role in determining the footprint, and an MHC-centric model,[20,34,44,45] in which the footprint is determined by the MHC, with the peptide having virtually no effect. These views are sometimes simplified as a "tail wagging the dog/dog wagging the tail" debate, with the dog being the MHC and the tail being the peptide. Some experimental results, such as the MHC mutation experiments of Felix et al.[30] and the alanine-substitution work of Conolly et al.,[22,31] have been cited as support for the peptide-centric idea. Other experiments, specifically the work of Colf et al.,[20] have been explained as support for the MHC-centric model.

Our findings serve as a synthesis and explanation of these apparently conflicting views. We show that, while CDR3 mutations do not necessarily influence the alloreactive contact footprint, peptide mutation, by contrast, can have an influence. The difference between the observed effects of these two kinds of mutations highlights the difference between influencing the TCR/peptide interactions by changing only the TCR's CDR3 residues and mutating the peptide itself, which is a more direct way to test the peptide-centric model. Our simulations reveal that the two experimental approaches are not equivalent, as mutations to the peptide can directly impact the MHC helices and thus affect the chemical surface to which the TCR binds in ways that mutations of the CDR3 loops cannot. However, even in the cases where we found that peptide mutations broadly affected the footprint, these effects were relatively localized compared to the difference between self- and allo-MHC footprints made by the 2C TCR.[20]

CONCLUSIONS

We thus predict that both MHC and peptide have a direct impact in determining the TCR/allo-pMHC footprint, with the peptide being able to "edit" the specific contacts after initial contact between the TCR and pMHC. One mechanism for this multilevel impact may involve the TCR "reading" the pMHC ligand in search of enough sufficiently favorable interactions. If enough interactions exist and the TCR/pMHC complex survives long enough, modest, specific rearrangements of the interface residues would occur to maximize the affinity.[8,29,49] This mechanism is consistent with our findings and is also consistent with diverse other findings, including those of MacDonald et al.,[47] because rearrangements after the initial scanning induced by the peptide could produce a similar final structure in initially different pMHC landscapes.

Looking forward, we believe that free energy simulations of TCR/allo-pMHC similar to those previously performed for TCR/self-pMHC[53−55] would be informative, providing more

detailed free energetic data, such as a systematic comparison of the relative contributions of peptide mutation and MHC changes on the TCR binding affinity. Most importantly, testing the predictions made by our simulations by obtaining crystal structures of the C8P and C8A systems (or some analogues) and performing analysis similar to our own with these structures will shed more light on the effect of the interplay between peptide and MHC on alloreactivity. We hope that our study will motivate such experiments.

■ ASSOCIATED CONTENT

Supporting Information. Quantitative information about the stability of the molecular dynamics situations and the effects of peptide mutation. This material is available free of charge via the Internet at http://pubs.acs.org.

■ AUTHOR INFORMATION

Corresponding Author

*E-mail: knam@fas.harvard.edu; arupc@mit.edu. Phone: +1 617 495 8997; +1 617 253 3890. Fax: +1 617 495 8755; +1 617 253 2272.

■ ACKNOWLEDGMENT

We thank Prof. Martin Karplus, Prof. Herman Eisen, and Dr. Abhishek Jha for their fruitful discussions and comments. Financial support was provided by NIAID Grant 5P01/AI071195/02 and an NIH Director's Pioneer Award to A.K.C.

■ REFERENCES

(1) Hogquist, K. A.; Jameson, S. C.; Bevan, M. J. *Curr. Opin. Immunol.* **1994**, *6*, 273.
(2) Jameson, S. C.; Hogquist, K. A.; Bevan, M. J. *Annu. Rev. Immunol.* **1995**, *13*, 93.
(3) Werlen, G.; Hausmann, B.; Naeher, D.; Palmer, E. *Science* **2003**, *299*, 1859.
(4) Starr, T. K.; Jameson, S. C.; Hogquist, K. A. *Annu. Rev. Immunol.* **2003**, *21*, 139.
(5) von Boehmer, H.; Aifantis, I.; Gounari, F.; Azogui, O.; Haughn, L.; Apostolou, I.; Jaeckel, E.; Grassi, F.; Klein, L. *Immunol. Rev.* **2003**, *191*, 62.
(6) Hogquist, K. A.; Baldwin, T. A.; Jameson, S. C. *Nat. Rev. Immunol.* **2005**, *5*, 772.
(7) Siggs, O. M.; Makaroff, L. E.; Liston, A. *Curr. Opin. Immunol.* **2006**, *18*, 175.
(8) Košmrlj, A.; Jha, A. K.; Huseby, E. S.; Kardar, M.; Chakraborty, A. K. *Proc. Natl. Acad. Sci. U.S.A.* **2008**, *105*, 16671.
(9) Huseby, E.; White, J.; Crawford, F.; Vass, T.; Becker, D.; Pinilla, C.; Marrack, P.; Kappler, J. *Cell* **2005**, *122*, 247.
(10) Huseby, E.; Crawford, F.; White, J.; Marrack, P.; Kappler, J. *Nat. Immunol.* **2006**, *7*, 1191.
(11) Lindahl, K. F.; Wilson, D. B. *J. Exp. Med.* **1977**, *145*, 508.
(12) Lynes, M. A.; Flaherty, L.; Michaelson, J.; Collins, J. J.; Rinchik, E. M. *J. Immunogenet.* **1984**, *11*, 189.
(13) Lechler, R. I.; Lombardi, G.; Batchelor, J. R.; Reinsmoen, N.; Bach, F. H. *Immunol. Today* **1990**, *11*, 83.
(14) Kaufman, C. L.; Gaines, B. A.; Ildstad, S. T. *Annu. Rev. Immunol.* **1995**, *13*, 339.
(15) Joyce, S.; Nathenson, S. G. *Immunol. Rev.* **1996**, *154*, 59.
(16) Le, N. T.; Chen, B. J.; Chao, N. J. *Cytotherapy* **2005**, *7*, 126.
(17) Hauben, E.; Bacchetta, R.; Roncarolo, M. G. *Cytotherapy* **2005**, *7*, 158.
(18) Felix, N. J.; Allen, P. M. *Nat. Rev. Immunol.* **2007**, *7*, 942.
(19) Nikolich-Zugich, J. *Nat. Immunol.* **2007**, *8*, 388.
(20) Colf, L. A.; Bankovich, A. J.; Hanick, N. A.; Bowerman, N. A.; Jones, L. L.; Kranz, D. M.; Garcia, K. C. *Cell* **2007**, *129*, 135.
(21) DeLano, W. *The PyMOL User's Manual*; 2002.
(22) Alexander-Miller, M. A.; Burke, K.; Koszinowski, U. H.; Hansen, T. H.; Connolly, J. M. *J. Immunol.* **1993**, *151*, 1.
(23) Basu, D.; Horvath, S.; Matsumoto, I.; Fremont, D. H.; Allen, P. M. *J. Immunol.* **2000**, *164*, 5788.
(24) Eisen, H. N. *Annu. Rev. Immunol.* **2001**, *19*, 1.
(25) Huseby, E. S.; Crawford, F.; White, J.; Kappler, J.; Marrack, P. *Proc. Natl. Acad. Sci. U.S.A.* **2003**, *100*, 11565.
(26) Panina-Bordignon, P.; Corradin, G.; Roosnek, E.; Sette, A.; Lanzavecchia, A. *Science* **1991**, *252*, 1548.
(27) Udaka, K.; Tsomides, T. J.; Eisen, H. N. *Cell* **1992**, *69*, 989.
(28) Garcia, K.; Adams, E. *Cell* **2005**, *122*, 333.
(29) Armstrong, K. M.; Piepenbrink, K. H.; Baker, B. M. *Biochem. J.* **2008**, *415*, 183.
(30) Felix, N. J.; Donermeyer, D. L.; Horvath, S.; Walters, J. J.; Gross, M. L.; Suri, A.; Allen, P. M. *Nat. Immunol.* **2007**, *8*, 388.
(31) Hornell, T. M.; Martin, S. M.; Myers, N. B.; Connolly, J. M. *J. Immunol.* **2001**, *167*, 4207.
(32) Garboczi, D.; Ghosh, P.; Utz, U.; Fan, Q.; Biddison, W.; Wiley, D. *Nature* **1996**, *384*, 134.
(33) Garcia, K. C.; Degano, M.; Pease, L. R.; Huang, M.; Peterson, P. A.; Teyton, L.; Wilson, I. A. *Science* **1998**, *279*, 1166.
(34) Ding, Y.; Baker, B.; Garboczi, D.; Biddison, W.; Wiley, D. *Immunity* **1999**, *11*, 45.
(35) Degano, M.; Garcia, K.; Apostolopoulos, V.; Rudolph, M.; Teyton, L.; Wilson, I. *Immunity* **2000**, *12*, 251.
(36) Hahn, M.; Nicholson, M. J.; Pyrdol, J.; Wucherpfennig, K. W. *Nat. Immunol.* **2005**, *6*, 490.
(37) Borbulevych, O. Y.; Piepenbrink, K. H.; Gloor, B. E.; Scott, D. R.; Sommese, R. F.; Cole, D. K.; Sewell, A. K.; Baker, B. M. *Immunity* **2009**, *31*, 885.
(38) Burrows, S.; Chen, Z.; Archbold, J.; Tynan, F.; Beddoe, T.; Kjer-Nielsen, L.; Miles, J.; Khanna, R.; Moss, D.; Liu, Y.; Gras, S.; Kostenko, L.; Brennan, R. M.; Clements, C. S.; Brooks, A. G.; Purcell, A. W.; McCluskey, J.; Rossjohn, J. *Proc. Natl. Acad. Sci. U.S.A.* **2010**, *107*, 10608.
(39) Reiser, J. B.; Darnault, C.; Guimezanes, A.; Gregoire, C.; Mosser, T.; Schmitt-Verhulst, A. M.; Fontecilla-Camps, J. C.; Malissen, B.; Housset, D.; Mazza, G. *Nat. Immunol.* **2000**, *1*, 291.
(40) Luz, J.; Huang, M.; Garcia, K.; Rudolph, M.; Apostolopoulos, V.; Teyton, L.; Wilson, I. *J. Exp. Med.* **2002**, *195*, 1175.
(41) Reiser, J. B.; Grégoire, C.; Darnault, C.; Mosser, T.; Guimezanes, A.; Schmitt-Verhulst, A. M.; Fontecilla-Camps, J. C.; Mazza, G.; Malissen, B.; Housset, D. *Immunity* **2002**, *16*, 345.
(42) Reiser, J.; Darnault, C.; Grégoire, C.; Mosser, T.; Mazza, G.; Kearney, A.; van der Merwe, P.; Fontecilla-Camps, J.; Housset, D.; Malissen, B. *Nat. Immunol.* **2003**, *4*, 241.
(43) Archbold, J.; Macdonald, W.; Miles, J.; Brennan, R.; Kjer-Nielsen, L.; McCluskey, J.; Burrows, S.; Rossjohn, J. *J. Biol. Chem.* **2006**, *281*, 34324.
(44) Jones, L. L.; Colf, L. A.; Bankovich, A. J.; Stone, J. D.; Gao, Y. G.; Chan, C. M.; Huang, R. H.; Garcia, K. C.; Kranz, D. M. *Biochemistry* **2008**, *47*, 12398.
(45) Jones, L.; Colf, L.; Stone, J.; Garcia, K.; Kranz, D. *J. Immunol.* **2008**, *181*, 6255.
(46) Gras, S.; Burrows, S. R.; Kjer-Nielsen, L.; Clements, C. S.; Liu, Y. C.; Sullivan, L. C.; Bell, M. J.; Brooks, A. G.; Purcell, A. W.; McCluskey, J.; Rossjohn, J. *Immunity* **2009**, *30*, 193.
(47) MacDonald, W. A.; Chen, Z.; Gras, S.; Archbold, J. K.; Tynan, F. E.; Clements, C. S.; Bharadwaj, M.; Kjer-Nielsen, L.; Saunders, P. M.; Wilce, M. C. J.; Crawford, F.; Stadinsky, B.; Jackson, D.; Brooks, A. G.; Purcell, A. W.; Kappler, J. W.; Burrows, S. R.; Rossjohn, J.; McCluskey, J. *Immunity* **2009**, *31*, 897.
(48) Karplus, M.; McCammon, J. *Nat. Struct. Biol.* **2002**, *9*, 646.
(49) Wu, L.; Tuot, D.; Lyons, D.; Garcia, K.; Davis, M. *Nature* **2002**, *418*, 552.

(50) Košmrlj, A.; Chakraborty, A. K.; Kardar, M.; Shakhnovich, E. *Phys. Rev. Lett.* **2009**, *103*, 068103.
(51) Eisen, H.; Chakraborty, A. *Proc. Natl. Acad. Sci. U.S.A.* **2010**, *107*, 22373.
(52) Brünger, A. *Prot. Struct. Funct. Genet.* **1988**, *4*, 148.
(53) Michielin, O.; Karplus, M. *J. Mol. Biol.* **2002**, *324*, 547.
(54) Wan, S. Z.; Coveney, P. V.; Flower, D. R. *J. Immunol.* **2005**, *175*, 1715.
(55) Zoete, V.; Michielin, O. *Proteins: Struct., Funct., Bioinf.* **2007**, *67*, 1026.
(56) MacKerell, A. D., Jr.; Bashford, D.; Bellott; Dunbrack, L., R.; Evanseck, J. D.; Field, M. J.; Fischer, S.; Gao, J.; Guo, H.; Ha, S.; Joseph-McCarthy, D.; Kuchnir, L.; Kuczera, K.; Lau, F. T. K.; Mattos, C.; Michnick, S.; Ngo, T.; Nguyen, D. T.; Prodhom, B.; Reiher, W. E.; Roux, B.; Schlenkrich, M.; Smith, J. C.; Stote, R.; Straub, J.; Watanabe, M.; Wiorkiewicz-Kuczera, J.; Yin, D.; Karplus, M. *J. Phys. Chem. B* **1998**, *102*, 3586.
(57) Jorgensen, W. L.; Chandrasekhar, J.; Madura, J. D.; Impey, R. W.; Klein, M. L. *J. Chem. Phys.* **1983**, *79*, 926.
(58) Brooks, B. R.; Bruccoleri, R. E.; Olafson, B. D.; States, D. J.; Swaminathan, S.; Karplus, M. *J. Comput. Chem.* **1983**, *4*, 187.
(59) Brooks, B. R.; Brooks, C. L., III; Mackerell, A. D., Jr.; Nilsson, L.; Petrella, R. J.; Roux, B.; Won, Y.; Archontis, G.; Bartels, C.; Boresch, S.; Caflisch, A.; Caves, L.; Cui, Q.; Dinner, A. R.; Feig, M.; Fischer, S.; Gao, J.; Hodoscek, M.; Im, W.; Kuczera, K.; Lazaridis, T.; Ma, J.; Ovchinnikov, V.; Paci, E.; Pastor, R. W.; Post, C. B.; Pu, J. Z.; Schaefer, M.; Tidor, B.; Venable, R. M.; Woodcock, H. L.; Wu, X.; Yang, W.; York, D. M.; Karplus, M. *J. Comput. Chem.* **2009**, *30*, 1545.
(60) Mackerell, A., Jr.; Feig, M.; Brooks, C., III. *J. Comput. Chem.* **2004**, *25*, 1400.
(61) van Gunsteren, W. F.; Berendsen, H. J. C. *Mol. Phys.* **1977**, *34*, 1311.
(62) Steinbach, P.; Brooks, B. *J. Comput. Chem.* **1994**, *15*, 667.
(63) Essmann, U.; Perera, L.; Berkowitz, M.; Darden, T.; Lee, H.; Pedersen, L. *J. Chem. Phys.* **1995**, *103*, 8577.
(64) Nosé, S. *J. Chem. Phys.* **1984**, *81*, 511.
(65) Hoover, W. G. *Phys. Rev. A* **1985**, *31*, 1695.
(66) Feller, S.; Zhang, Y.; Pastor, R.; Brooks, B. *J. Chem. Phys.* **1995**, *103*, 4613.
(67) Eisen, H. N.; Sykulev, Y.; Tsomides, T. J. *Adv. Protein Chem.* **1996**, *49*, 1.
(68) Kageyama, S.; Tsomides, T. J.; Fukusen, N.; Papayannopoulos, I.; Eisen, H. N.; Sykulev, Y. *J. Immunol.* **2001**, *166*, 3028.
(69) Kranz, D. M.; Sherman, D. H.; Sitkovsky, M. V.; Pasternack, M. S.; Eisen, H. N. *Proc. Natl. Acad. Sci. U.S.A.* **1984**, *81*, 573.
(70) Sha, W. C.; Nelson, C. A.; Newberry, R. D.; Kranz, D. M.; Russell, J. H.; Loh, D. Y. *Nature* **1988**, *336*, 73.
(71) Humphrey, W.; Dalke, A.; Schulten, K. *J. Mol. Graphics* **1996**, *14*, 33.